DOE/NASA/20485-79/4
NASA TM-79209

DYNAMIC ANALYSIS OF A PHOTOVOLTAIC POWER SYSTEM WITH BATTERY STORAGE CAPABILITY

Walter C. Merrill, Ronald J. Blaha,
and Roy L. Pickrell
National Aeronautics and Space Administration
Lewis Research Center

July 197

Prepared for
U.S. DEPARTMENT OF ENERGY
Energy Technology
Distributed Solar Technology Division

DOE/NASA/20485-79/4
NASA TM-79209

DYNAMIC ANALYSIS OF A PHOTOVOLTAIC POWER SYSTEM WITH BATTERY STORAGE CAPABILITY

Walter C. Merrill, Ronald J. Blaha,
and Roy L. Pickrell
National Aeronautics and Space Administration
Lewis Research Center
Cleveland, Ohio 44135

July 1979

Work performed for
U.S. DEPARTMENT OF ENERGY
Energy Technology
Distributed Solar Technology Division
Washington, D.C. 20545
Under Interagency Agreement DE-AI01-79ET20485

SUMMARY

A photovoltaic power system with a battery storage capability is analyzed. A dual battery current control concept is proposed, which enables the battery to either supply or accept power depending upon system environment and load conditions. A simulation of the power system, including the battery current control, is developed and evaluated. The evaluation demonstrated the viability of the battery control concept to switch the battery from a charge to discharge mode and back as required by load and environmental conditions. An acceptable system operation is demonstrated over the entire insolation range. Additionally, system sensitivity, bandwidth, and damping characteristics of the battery control are shown to be acceptable for a projected hardware implementation.

INTRODUCTION

Recently much emphasis has been placed on the conversion of solar energy to more usable energy forms. One method is the direct conversion of solar insolation to a dc voltage and current by the use of solar cells. This dc power can then be "inverted" to ac power compatible with various ac machines and loads.

The Terrestial Photovoltaic Project Office, as part of a DOE effort, is developing a 10 kVA Inverter/Controller subsystem for testing in a Photovoltaic Power System (PPS) at the Lewis Research Center (LeRC). The purpose of the combined system (PPS) is to investigate the application potential of photovoltaic power sources to supplement and/or replace conventional energy supplies. A description of the PPS and its operation can be found in reference 1.

In a true "stand alone - hands off" continuous mode of operation, the PPS will require energy storage capability. This capability should sustain loads during periods of low solar insolation and accept excess available power from the solar array during peak sunlight hours in order to optimize relatively expensive solar array power capability. Such storage capability is typically accomplished with a battery. Simplistic battery storage systems have been designed for low power PPS installations by simply shunting the battery across the Solar Array (SA) output terminals. Optimization of these designs for large changes in solar insolation and operating temperature is difficult. Also, the battery can be subjected to possible damage due to over change and charge depletion. This report includes a more sophisticated Battery Current Control (BCC) concept, as part of a total PPS system, as an alternative to this simplistic design.

The total PPS system, as shown in figure 1, consists of six major blocks: (1) an array of solar cells; (2) the 10 kVA dc to ac power inverter (PI); (3) the power system controller (PSC); (4) the pilot sensor array; (5) the dc load control (DCC); and (6) the battery current control and battery. The solar array directly converts solar insolation into dc power. The inverter transforms this dc power to 60 hertz ac power compatible with most electrically driven machines.

The power required from the dc bus is determined by the dedicated loads and system losses. Should the power generated by the SA be insufficient to meet the demand, the PSC signals the BCC and power is transferred from the battery to the dc bus to make up the power deficit. Should the power generated by the SA exceed the demand, the PSC signals the BCC and excess power is transferred from the dc bus to the battery. The pilot sensor array supplies the PSC with an approximate maximum power operating voltage for the solar array. If the battery is in a state of full charge, a signal is sent to the DCC and the excess power is dissipated through a resistance load. Functionally, the BCC operates as in figure 2. The two dc to dc converters act as power switches to direct the flow to and from the battery. Additionally, they act as power conditioning or matching devices, since at any instant of time the dc bus voltage and current can differ from the battery voltage and current.

The system of figure 1 was simulated using an analog computer by formulating a model of the BCC, battery, and controls of figure 2 and combining it with the system model described in reference 1. Appropriate modifications were made to the PSC to handle additional control functions. This report describes the model used for the analog computer simulation of the combined PPS and gives the results of several experiments performed on this simulation. These experiments were used to evaluate system operation for various insolation levels, load levels, and control configurations. This report begins with a detailed description of the PPS and its components.

Photovoltaic Power System Description

For the simulation the PPS was modeled as shown in figure 3. A list of symbols is given in appendix A and a summary of model equations is given in appendix B. Dynamically, the important elements are: (1) the solar array; (2) the power inverter; (3) the power system controller; (4) the two 0.021 farad filter capacitors; (5) the battery current charge and discharge converters; and (6) the battery. In this model the pilot sensor array function is obtained from the solar array open circuit voltage data model. Figure 3 also indicates important system variables.

Energy conversion is accomplished by the solar array. Impinging direct solar insolation is changed to a dc voltage and current. The power inverter "inverts" dc power at varying levels of voltage and current to ac power at a constant voltage magnitude. The charge converter "converts" the varying dc voltage and current of the dc bus to a dc voltage and current at the battery, compatible with the battery state of charge (SOC) and the power transfer requirement. The discharge converter performs exactly the same function as the charge converter, only the direction of the power (current) flow is reversed. The power inverter and the charge converters require pulsating dc input currents. The input filter capacitors isolate the array from these pulsating dc currents. Because of the storage characteristics of the battery, no filter capacitor is needed at the input of the discharge converter. The operating point voltage of the SA is determined by the pilot sensor array for the PSC to maximize available power at any instant of time. Each component model is now described in detail.

Solar Array

The solar array consists of several hundred interconnected solar cells. The current-voltage characteristics for each cell for different solar insolation levels and ambient temperatures are determined experimentally and are presented in figure 4. The entire array consists of 80 parallel connected strings of solar cells with 480 series connected cells per string. Therefore a total solar array characteristic could be obtained by a simple scaling of the individual cell characteristic as shown in figure 4. The ordinate intercept value of each curve is called the short circuit current, $I_{SA,N}$, and the abscissa intercept value the open circuit voltage, $E_{SA,N}$. A normalization of each curve by its open circuit voltage and short circuit current values yields a single curve representative of all temperatures and insolation conditions (fig. 5). This representation is convenient for usage in a system simulation since only one nonlinear curve need be programmed.

Power System Control

It was determined (ref. 1) that maximum power from the SA is obtained when

$$E_{SA} = 0.7823\, E_{SA,N} \tag{1}$$

One control task of the PSC is to maintain the relation of (1) by controlling the flow of power (current) from the SA to the combined load of the battery, the dc load, and the inverter. However, operation of the dc load control was not analyzed in this study. A second control function of the PSC is the regulation of the magnitude of the inverter output voltage to 240 $\sqrt{2}$ volts. Although the hardware to accomplish this second control function is actually part of the power inverter, conceptually it will be included with the PSC in this study. The PSC is summarized in block diagram form in figure 6. In figure 6(a) the power inverter control voltage, $E_{P, CONT}$, is generated by a proportional-integral control that maintains the inverter output voltage, e_A, magnitude at 240 $\sqrt{2}$ volts. The dynamics of the measurement of $|e_A|$ for the feedback signal was not considered in this report to simplify the study. No appreciable impact on system operation by these dynamics is expected. In figure 6(b) the dc bus feedback voltage, E_{BUS}, is filtered by a three pole, 40 hertz, Butterworth filter to remove 120 hertz noise and compared to the reference voltage of (1). The error signal is filtered by a 500 hertz, single pole, low pass filter to remove high frequency noise. The filtered error signal then drives a proportional-integral control to generate the power control voltage, E_{CONT}.

Once the power control voltage has been generated, the charge and discharge control voltages are determined from it. The basic BCC scheme is

$$E_{C, CONT} = \begin{cases} 0.8 + 0.2\, E_{CONT} & \Delta I > 0 \\ 0 & \Delta I \leq 0 \end{cases} \tag{2}$$

$$E_{D, CONT} = \begin{cases} 0.8 - 0.2\, E_{CONT} & \Delta I < 0 \\ 0 & \Delta I \geq 0 \end{cases} \tag{3}$$

where

$$\Delta I = I_{SA} - I_P \tag{4}$$

Several modifications to this scheme were evaluated to determine if control improvements could be made and to study the effect of various hardware limitations in the implemented control. These modifications will be discussed in the results section.

Power Inverter

The power inverter transforms dc input power generated by the solar array into single phase ac power compatible with most electrical machines. Conversion is accomplished by approximating the desired sinusoidal inverter output voltage by a preprogrammed sequence of dc pulses. The resultant sequence is filtered to remove high order harmonics. Additionally, the inverter acts as an impedance matching device. The variable voltage and current of the dc bus is matched to the ac load at a constant output voltage. For the model used in the simulation, the inverter is considered to be an ideal power conversion device with dc power in equal to ac power out. The inverter losses and the output filtering are lumped together with the load impedance. Frequency information is not used explicitly in the model. Therefore only the magnitude and phase of the variables on the output side of the inverter are of interest. Inverter output voltage regulation is accomplished by adjusting $E_{P, CONT, F}$. This control signal adjusts the magnitude of the generated voltage and, as a result, the line current to maintain the output or load voltage. The power inverter and load impedance is shown in block form in figure 3.

Power Converters

A power converter couples a dc power source to a dc power load where both source and load operate at differing voltage and current levels.

The charge and discharge converters are identical in operation. They both couple the battery and the dc bus. Only the direction of current flow is different. Therefore, the model used for each device will be the same with appropriate changes in variable names. Conceptually, the operation of the converter is modeled exactly as the inverter, i.e., power in equals power out at any instant of time. The difference is that output power is now a dc rather than ac power. Control is established by either $E_{C, CONT, F}$ or $E_{D, CONT, F}$. The magnitude of the output voltage is directly modulated by the control voltage. The losses associated with the converter are modeled by a diode and two resistors. The charge and discharge converters with the loss elements are shown in figure 3.

Battery

The model for the chemical battery assumes that the state of the battery can be completely described at any time by the voltage across the battery terminals, the current through the battery, and the battery state of charge. This model is characterized by the current-voltage curves in figure 7 which are parameterized by the SOC for a typical lead antimony/lead calcium storage battery. To facilitate analog computer simulation, the curves of figure 7 were approximated by straight line segments. The reciprocal of the slopes and "x-axis" intercepts (battery voltage at zero current) of these segments for both charge and discharge conditions are plotted in figures 8 and 9 against SOC. This enables battery voltage, E_B, to be calculated as a function of battery current, I_B, and SOC as in equations (B1) to (B10). Thus two univariate functions are programmed into the analog computer to find E_B, which is simpler than programming a single bivariate function. Note that in figure 7 two different approximations were used for the 90% SOC charge characteristic. The dashed line more closely approximates the slope of the actual curve at higher voltages. No appreciable difference was detected in any of the simulation tests, however, using these different approximations.

The battery selected for the system has a 100 A-hr rating. This rating determines the rate of charge and discharge of the battery. The battery SOC can be expressed as

$$D\{SOC\} = K_B I_B$$

where SOC is percent of full charge, I_B is battery current, and K_B is rating constant. Thus, if I_B is constant and the battery is initially uncharged, then

$$SOC = K_B I_B t$$

where t is in seconds and full charge is 100 A-hr or 3.6×10^5 A-sec. Letting

$$I_B t = 3.6\times10^5 \text{ A-sec}$$

then

$$K_B = \frac{100\%}{3.6\times10^5 \text{ A-sec}} = 2.778\times10^{-4} \frac{\%}{\text{A-sec}}$$

Simulation Results

To evaluate the battery storage concept and to determine the best charge-discharge control strategy, several simulation experiments were made. These experiments studied PPS dynamic operation for changes in solar insolation, battery state of change, and system load. A basic set of six experiments called "runs" were used to perform the evaluations. The six basic runs are described in figure 10. Two types of transients are used, the cloud cover/clear transient and the load variation transient. In this report a "cloud cover" transient is simulated by a change in solar insolation from 100 mW/cm^2 (cloudless) to 6.5 mW/cm^2 in 5 seconds. This is accomplished in the simulation by decreasing $E_{SA,N}$ linearly from its 100 mW/cm^2 value to its 6.5 mW/cm^2 value. The normalizing or short circuit current is then varied according to the equation

$$I_{SA,N} = 1.034\ E_{SA,N} - 205.06$$

A "cloud clear" transient is determined in exactly the same way except that insolation is increased from 6.5 to 100 mW/cm^2.

The second transient type is the load variation transient. This transient simulates an instantaneous step change in system load impedance. Experiments for both transient types are performed at a 30 and 95% SOC to simulate a discharged and fully charged condition. Also, the system is assumed to operate at a constant 55° C ambient temperature. The six runs were selected to investigate worst case conditions for the system. For example, run 6 conditions include minimum available power from SA (6.5 mW/cm^2) and the battery (30% SOC) and an instaneous change from a minimum to maximum power demand (1.0 to 10.0 kW load).

There are four different groups of experiments. Each group included all six run conditions. Since there is a large number of experiments, the simulation results have been summarized in figure 11 according to group, run, and figure number. This will facilitate comparison between similar transients. Additional comments are included to indicate modifications made to the BCC. Note that not every run in every group is presented. For example, results corresponding to run 3

are not presented for any group. These results, run 3 and all other omitted tests, although completed are not included here for two reasons. First, this limits the total number of presented results; and second, these results are, in every case, well behaved and do not demonstrate any important or unusual findings.

The first set of runs was completed for the BCC of equations (2) to (4). This is the basic charge control system and this set of runs is called group 1. Transient results were recorded for 15 pertinent system variables for all experiments. These six runs served as a baseline for the remaining data. All recorded traces indicated that the total system is well behaved. Large transients are seen in the control signals and in run 6, $E_{P,CONT}$, exceeds design limits when the steps in system load are encountered (fig. 12). Figures 13 and 14 summarize how well the SA operating line is maintained during cloud cover and clear transients. Perfect control would be a straight line intercepting each SA characteristic at 0.7823 of its open circuit voltage (approximate maximum power operating point). (Note that in future figures of this type the SA characteristics are omitted.) The digressions from the operating line occur when the BCC changes the battery from one mode to another, either charge or discharge. Much of this digression is directly related to the integral control action of the PSC. Figure 13 corresponds to runs 1 and 2 while figure 14 corresponds to runs 4 and 5.

The effect of the two low pass filters that follow the BCC (fig. 6) was investigated. Nominally, as in the group 1 transients, the low pass filters were single pole with a 1.0 hertz characteristic. In group 2 the low pass filters were changed to 0.5 hertz filters. Again the basic set of six runs was simulated. The operating line characteristics are given in figure 15 for runs 1 and 2 and figure 16 for runs 4 and 5. In all cases the group 1 control action more closely approximates the ideal control action than group 2. The system of group 2 has longer but smoother transients than that of group 1. This is a direct result of lower control system bandwidth and additional damping. This additional damping is beneficial to system stability and the resultant control degradation is acceptable. Thus the implementation of the 0.5 hertz characteristic is included in the studies of group 3. BCC control of equations (2) to (4) requires measurement of I_{SA} and I_P. Since these both can be large dc currents, measurement limitations in the hardware are to be expected. The transients of group 3 study the separate effects of an active hysteresis and a ±5% measurement error, typical measurement effects, on the measurement of ΔI of equation (4). The hysteresis characteristic is shown in figure 17 and the measurement error modification to equation (4) is

$$\Delta I = (1.0 \pm 0.05)(I_{SA} - I_P) \tag{5}$$

Figures 18 and 19 show the effects of the hysteresis on control performance for a cloud cover and cloud clear, respectively. Each figure compares no hysteresis (w = 0.0 A) to hysteresis widths w = 2.6 A and w = 2.5 A. Note that for a cloud clear transient with w = 2.5 A, the BCC voltage saturated and control over the PPS was lost. Such an instability could result in an unacceptable SA condition and a system shutdown and must be avoided.

Figures 20 and 21 show the effects of the measurement error of equation (5) on the PPS. Again cloud cover and cloud clear transients are shown that compare control performance for no error and ±5% measurement error operation. Figure 21 shows a loss of system control for a -5% error that would be unacceptable.

The system control problems highlighted in the group 3 transients indicated the need for an alternate BCC control strategy. An alternative, or modified control, was devised that was similar to the basic control. In the modified version of the BCC, the switching function that changes the battery mode of operation is now E_{CONT} rather than ΔI. The modified BCC in equation form is

$$E_{C,CONT} = \begin{cases} 0.8 + 0.2\,E_{CONT} & E_{CONT} > 0 \\ 0 & E_{CONT} \leq 0 \end{cases} \tag{6}$$

$$E_{D,CONT} = \begin{cases} 0.8 - 0.2\,E_{CONT} & E_{CONT} < 0 \\ 0 & E_{CONT} \geq 0 \end{cases} \tag{7}$$

The basic set of runs was completed for the PPS with the modified BCC. This set of runs is called group 4. The BCC filter frequency breakpoint characteristics for this group are again 1.0 hertz. Overall system control was acceptable for all runs except runs 1 and 2. From the simulated responses, it is apparent that more damping would be required in the actual system. The runs 1 and 2 operating line characteristics of group 4 (fig. 22) show a loss of control and limit cycling at low insolation levels. Runs 4 and 5 (fig. 23) show some harsh transients, but overall system operation is acceptable. The control performance indicated in runs 1 and 2, however, is not acceptable even though the loss of control occurs at a low insolation level. Note in figure 24 (the time history of run 1) the sustained oscillation of several system voltages and currents. It was discovered that the range of

$E_{D,CONT}$ was the limiting factor in the above control problem. A slight modification of the BCC to

$$E_{C,CONT} = \begin{cases} 0.8 + 0.2\,E_{CONT} & E_{CONT} > 0 \\ 0 & E_{CONT} \leq 0 \end{cases} \quad (8)$$

$$E_{D,CONT} = \begin{cases} 0.75 - 0.2\,E_{CONT} & E_{CONT} < 0 \\ 0 & E_{CONT} \geq 0 \end{cases} \quad (9)$$

which lowers the range of the discharge converter voltage eliminated the loss of control at low insolation levels as is demonstrated in figure 25 which is also included in group 4. Some cycling remains, but it damps out in less than 2 seconds. However, overall system control is maintained even under a low insolation condition.

With the updated BCC no current measurements are required. Thus, the hysteresis and measurement error problems are avoided. Additionally, since E_{CONT} is generated internally to the PSC, a good signal will be available for control. In spite of this, a cloud cover transient was run with a 20% deadband on E_{CONT} ($\pm 10\%$ centered on $E_{CONT} = 0.0$). The deadband, which is much larger than would be anticipated in practice, has a small effect on system performance as is seen in figure 26.

CONCLUSIONS

A simulation of a PPS with battery storage was developed. An analysis using this simulation demonstrated the viability of a BCC concept that effectively switches the battery from a charge to a discharge mode as required by system load and environmental conditions. A modification of the BCC concept to incorporate voltage rather than current feedback was shown to acceptably control the PPS at all but very low insolation levels. A second modification to the BCC which lowered the voltage range of the discharge converter enabled the PPS to operate at even these low insolation levels. Additionally, it was demonstrated that by reducing control system bandwidth via the BCC filters, that more overall system damping could be obtained. Finally, it was shown that the control implementation was reasonably insensitive to limitations in the expected hardware control implementation.

APPENDIX A

SYMBOLS

D	derivative operator, sec^{-1}
D{ }	derivative operator, sec^{-1}
E	dc voltage, V
e	ac voltage, V (60 Hz)
f( )	system function
I	dc current, A
i	ac current, A (60 Hz)
K	battery rating constant, %/A sec
M	reciprocal slope
SOC	state of charge, %
V	resistor voltage, V
w	hysteresis width, A
Z	ac load impedance, ohms
θ	load impedance phase angle, rad
| |	magnitude

Subscripts:

A	inverter output
B	battery
BUS	dc bus
C	charge
CONT	control
D	discharge
ERR	error
F	filtered
IN	hysteresis input

INT	intercept
L	load
N	normalizing
OUT	hysteresis output
P	power inverter
REF	reference
SA	solar array
SET	set point
1	converter output

APPENDIX B

MODEL EQUATIONS

Battery:

$$I_B = I_{B,C} - I_{B,D} \tag{B1}$$

$$E_B = f_B(I_B, SOC) \tag{B2}$$

$$D\{SOC\} = K_B I_B \tag{B3}$$

Battery Map:

$$M_C = f_{M,C}(SOC) \tag{B4}$$

$$M_D = f_{M,D}(SOC) \tag{B5}$$

$$E_{B,INT,C} = f_{INT,C}(SOC) \tag{B6}$$

$$E_{B,INT,D} = f_{INT,D}(SOC) \tag{B7}$$

$$E_{B,C} = E_{B,INT,C} + M_C I_B \tag{B8}$$

$$E_{B,D} = E_{B,INT,D} + M_D I_B \tag{B9}$$

$$E_B = \begin{cases} E_{B,C}, & I_B > 0 \\ E_{B,D}, & I_B < 0 \end{cases} \tag{B10}$$

Solar Array:

$$\frac{I_{SA}}{I_{SA,N}} = f_1\left(\frac{E_{SA}}{E_{SA,N}}\right) \tag{B11}$$

$$I_{SA,N} = 1.034\ E_{SA,N} - 205.06 \tag{B12}$$

DS Bus:

$$E_{BUS} = E_{SA} \tag{B13}$$

$$D\{E_{BUS}\} = \frac{I_{SA} - I_P - I_C + I_D}{0.042} \tag{B14}$$

Power Inverter:

$$I_P = \frac{|e_A||i_A| \cos\theta}{2\ E_{BUS}} \tag{B15}$$

$$|e_A| = 0.4243\ E_{BUS} E_{P,CONT,F} \tag{B16}$$

Inverter Load:

$$|i_A| = |e_A| / |Z| \tag{B17}$$

$$\theta = \angle Z \tag{B18}$$

$$i_A = |i_A| \angle 0 \tag{B19}$$

Battery Charge Converter:

$$E_C = E_{C,CONT,F} E_{BUS} \tag{B20}$$

$$I_C = I_{B,C,1} = I_{B,C} + \frac{E_C}{730} \tag{B21}$$

$$I_{B,C} = \begin{cases} 10(V_C), & V_C \geq 0 \\ 0, & V_C < 0 \end{cases} \tag{B22}$$

$$V_C = E_C - E_B - 1.0 \tag{B23}$$

Battery Discharge Converter:

$$E_D = E_{D,CONT,F} E_B \tag{B24}$$

$$I_{B,D} = \frac{E_D I_{D,1}}{E_B} \tag{B25}$$

$$I_{D,1} = I_D + \frac{E_D}{576} \tag{B26}$$

$$I_D = \begin{cases} 10(V_D), & V_D \geq 0 \\ 0, & V_D < 0 \end{cases} \tag{B27}$$

$$V_D = E_D - E_{BUS} - 1.0 \tag{B28}$$

Power System Control:

$$(0.00794\ D + 1)\left[\left(\frac{D}{126}\right)^2 + \left(\frac{D}{126}\right) + 1\right] E_{BUS,F} = 0.0156\ E_{BUS} \tag{B29}$$

$$D\left[0.318(10^{-3})D + 1\right] E_{CONT} = 5(D + 1)(E_{BUS,F} - E_{REF}) \tag{B30}$$

$$E_{REF} = 0.0125\, E_{SA,N} \tag{B31}$$

$$D\{E_{P,CONT,F}\} = \frac{E_{P,CONT} - E_{P,CONT,F}}{0.159} \tag{B32}$$

$$E_{P,CONT} = E_{ERR} + \int_0^+ E_{ERR}\,dt \tag{B33}$$

$$E_{ERR} = |e_A|_{SET} - |e_A| \tag{B34}$$

Battery Current Control:

$$D\{E_{C,CONT,F}\} = \frac{E_{C,CONT} - E_{C,CONT,F}}{0.159} \tag{B35}$$

$$D\{E_{D,CONT,F}\} = \frac{E_{D,CONT} - E_{D,CONT,F}}{0.159} \tag{B36}$$

$$E_{C,CONT} = \begin{cases} 0.8 + 0.2\, E_{CONT} & X > 0 \\ 0 & X \leq 0 \end{cases} \tag{B37}$$

$$E_{D,CONT} = \begin{cases} Y - 0.2\, E_{CONT} & X < 0 \\ 0 & X \geq 0 \end{cases} \tag{B38}$$

Basic BCC Version:

$$\begin{aligned} X &= \Delta I = I_{SA} - I_P \\ Y &= 0.8 \end{aligned} \tag{B39}$$

Updated BCC Version:

$$\begin{aligned} X &= E_{CONT} \\ Y &= 0.8 \end{aligned} \tag{B40}$$

Modified BCC Version:

$$X = E_{CONT}$$
$$Y = 0.75 \qquad \text{(B41)}$$

REFERENCE

1. Merrill, Walter C.; Blaha, Ronald J.; and Pickrell, Roy L.: Performance and Stability Analysis of a Photovoltaic Power System. DOE/NASA/1022-78/30, NASA TM-78880, 1978.

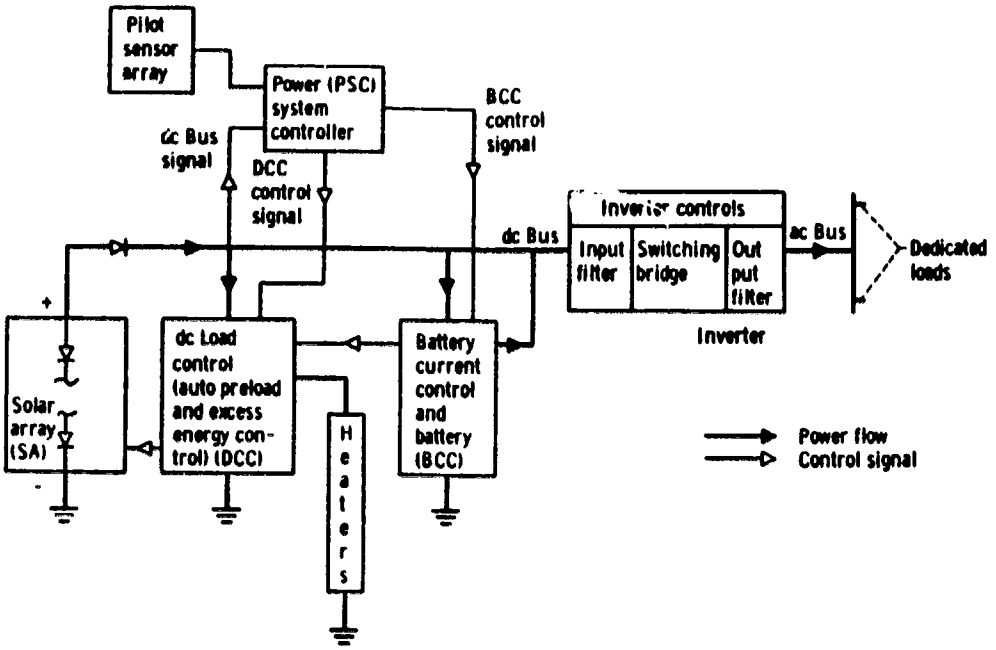

Figure 1. - 10 KVA photovoltaic power system stand alone mode.

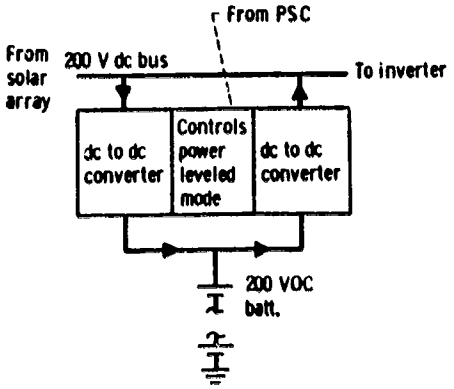

Figure 2. - BCC functional block diagram.

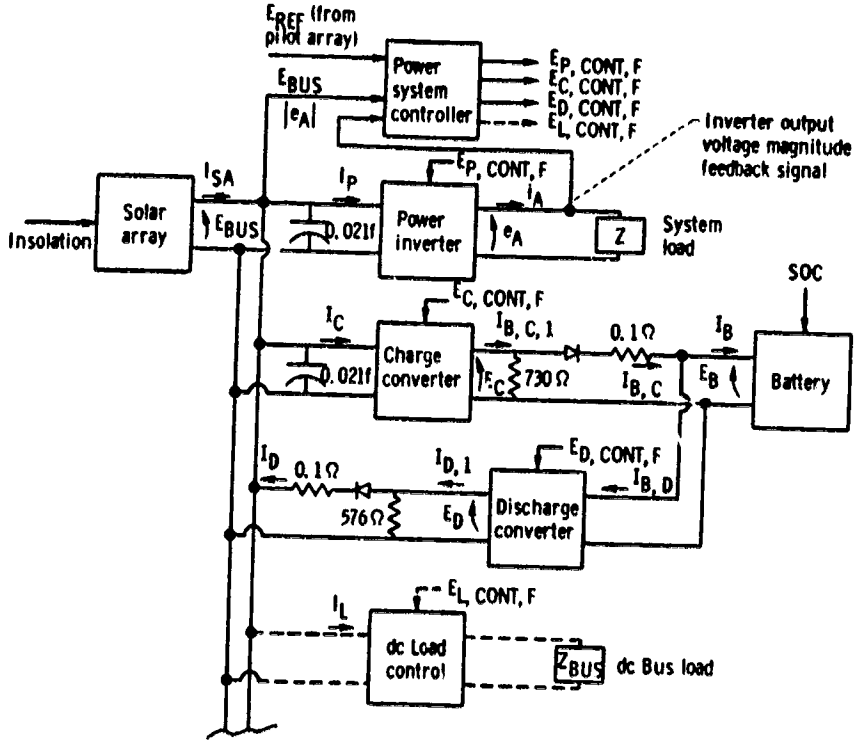

Figure 3. - Photovoltaic power system model block diagram.

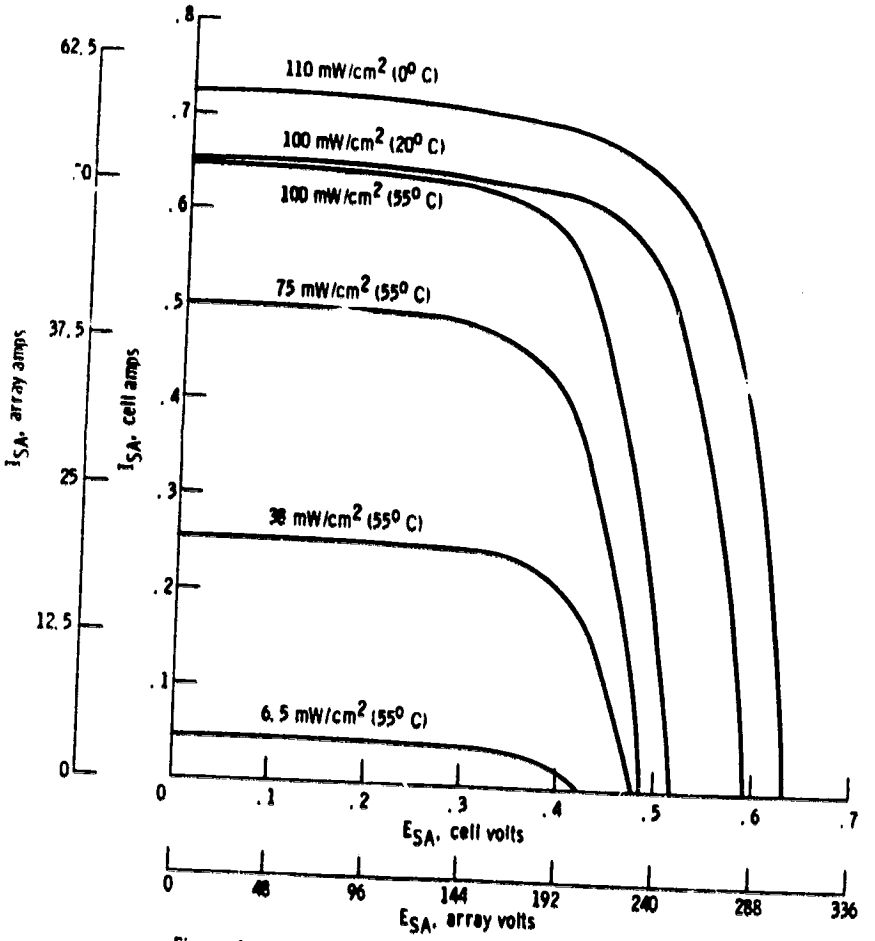

Figure 4. - Solar cell and solar array voltage-current characteristics.

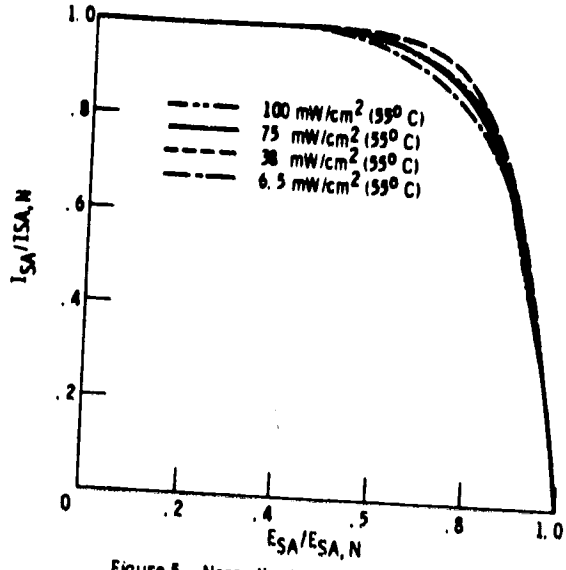

Figure 5. - Normalized solar array characteristic.

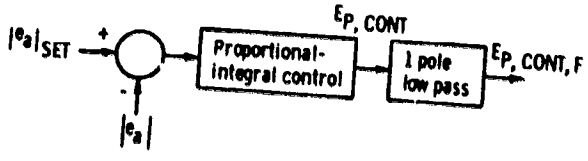

(a) Power inverter control.

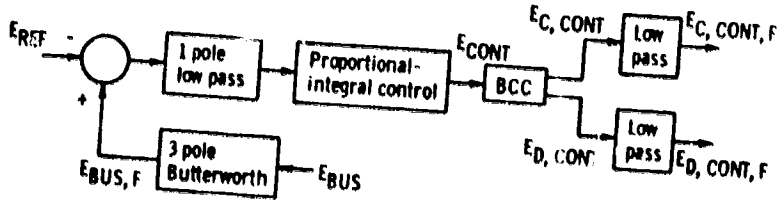

(b) Charge-discharge converter control.

Figure 6. - Power system control block diagram.

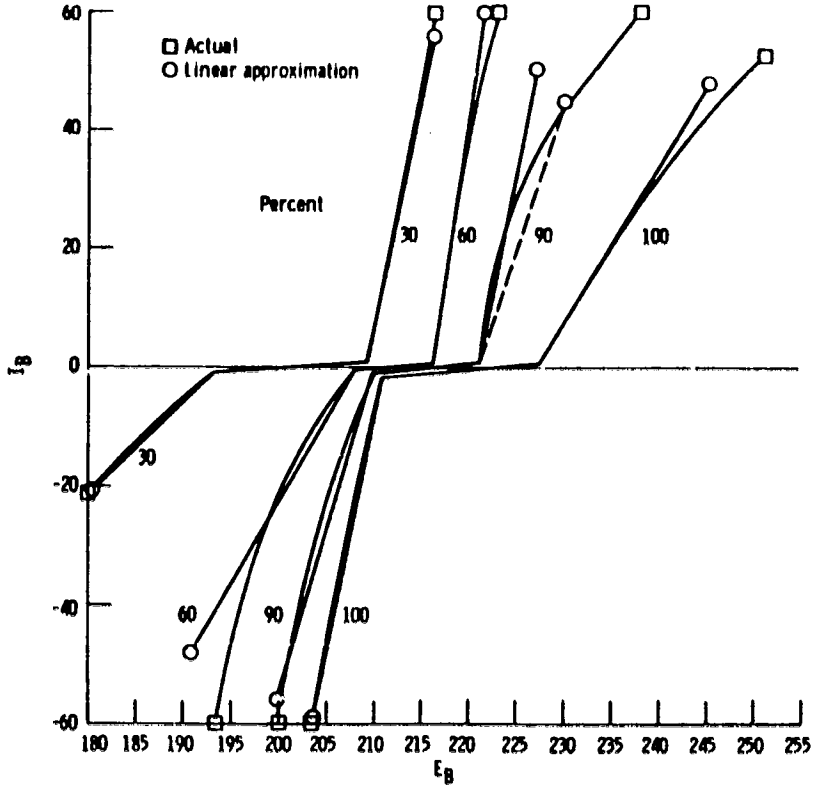

Figure 7. - Battery current-voltage characteristic-parameterized by SOC.

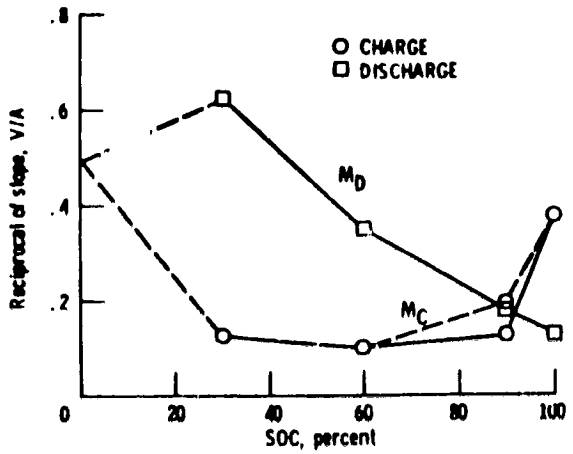

Figure 8. - Slope vs SOC.

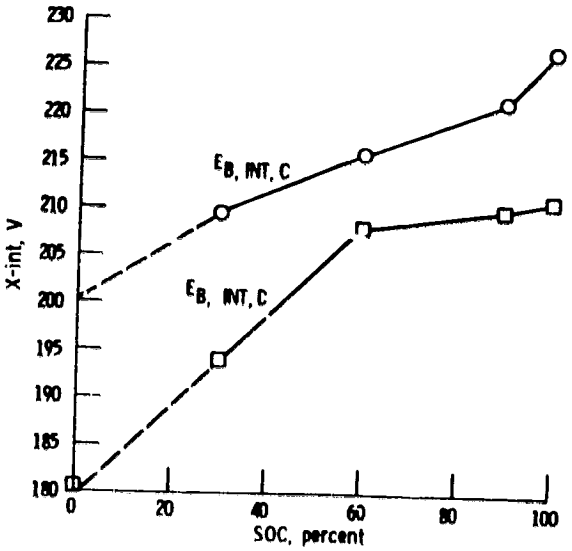

Figure 9. - "X-axis" intercept vs SOC.

Run no.	Insolation, mW/cm^2	SOC, percent	Load, kW
1	Cloud cover	95	1.0
2	Cloud clear	95	1.0
3	100	95	1 to 10 and 10 to 1 (Step changes)
4	Cloud cover	30	5.0
5	Cloud clear	30	5.0
6	6.5	30	10 to 1 and 1 to 10 (Step changes)

Figure 10. - Basic experiment description.

Group no.	Run no.	Figure no.	Figure type*	Modifications
1	6	12	T. T.	None (basic BCC)
	1 & 2	13	O. L.	None (basic BCC)
	4 & 5	14	O. L.	None (basic BCC)
2	1 & 2	15	O. L.	0.5 Hz BCC filter characteristics
	4 & 5	16	O. L.	0.5 Hz BCC filter characteristics
3	4	18	O. L.	0.5 Hz BCC; ω = 0, 2.0, 2.5 A
	5	19	O. L.	0.5 Hz BCC; ω = 0, 2.0, 2.5 A
	4	20	O. L.	0.5 Hz BCC; $(1 + 0.05)\Delta I$
	5	21	O. L.	0.5 Hz BCC; $(1 \mp 0.05)\Delta I$
4	1 & 2	22	O. L.	Updated BCC
	4 & 5	23	O. L.	Updated BCC
	1	24	T. T.	Updated BCC
	1	25	T. T.	Modified BCC
	1	26	T. T.	Modified BCC; 20 percent deadband

*O. L. - Operating line; T. T. - Time trace.

Figure 11. - Simulation results summary.

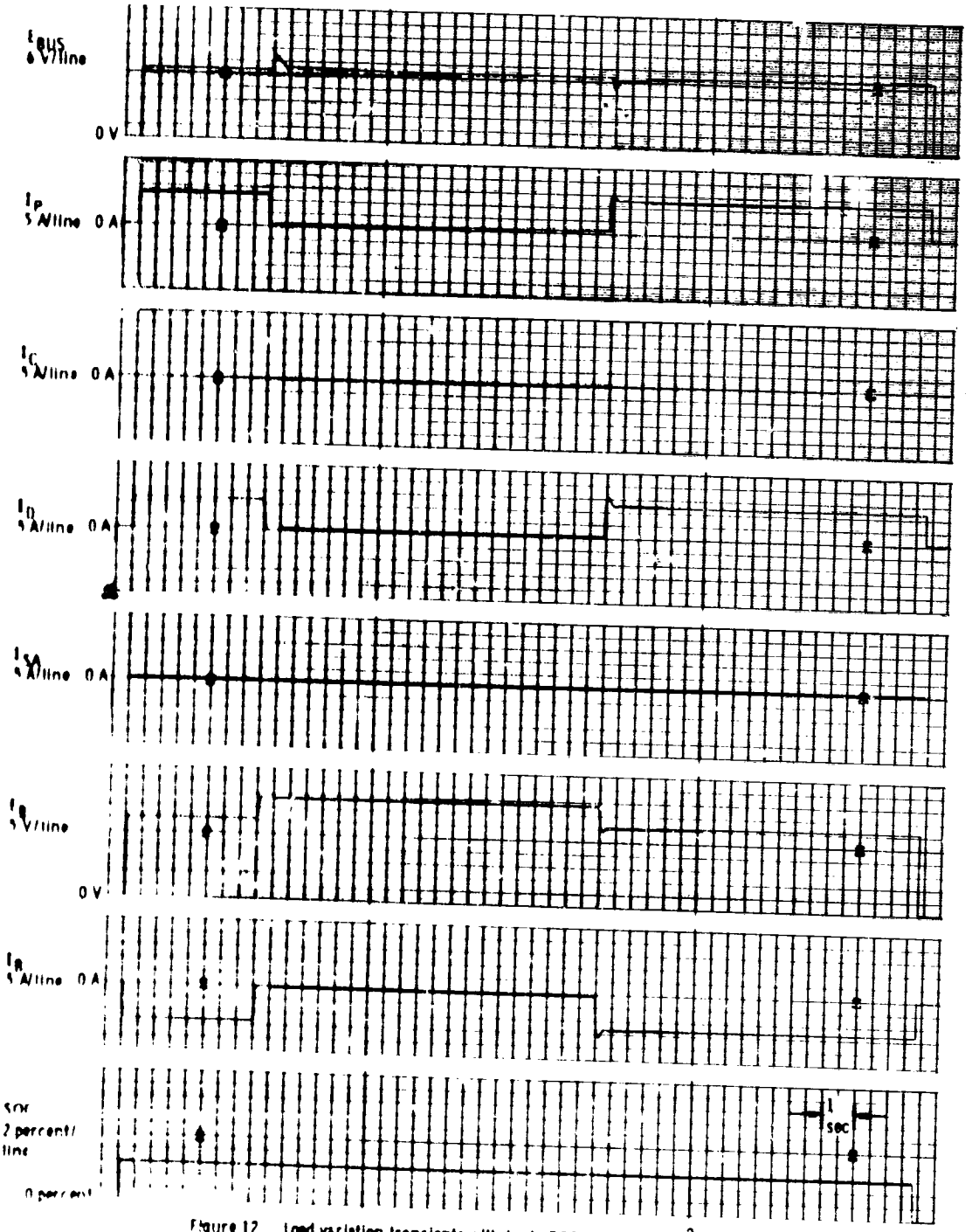

Figure 17 Load variation transients with basic BCC at 6.5 mW/cm^2 at 30 percent SOC.

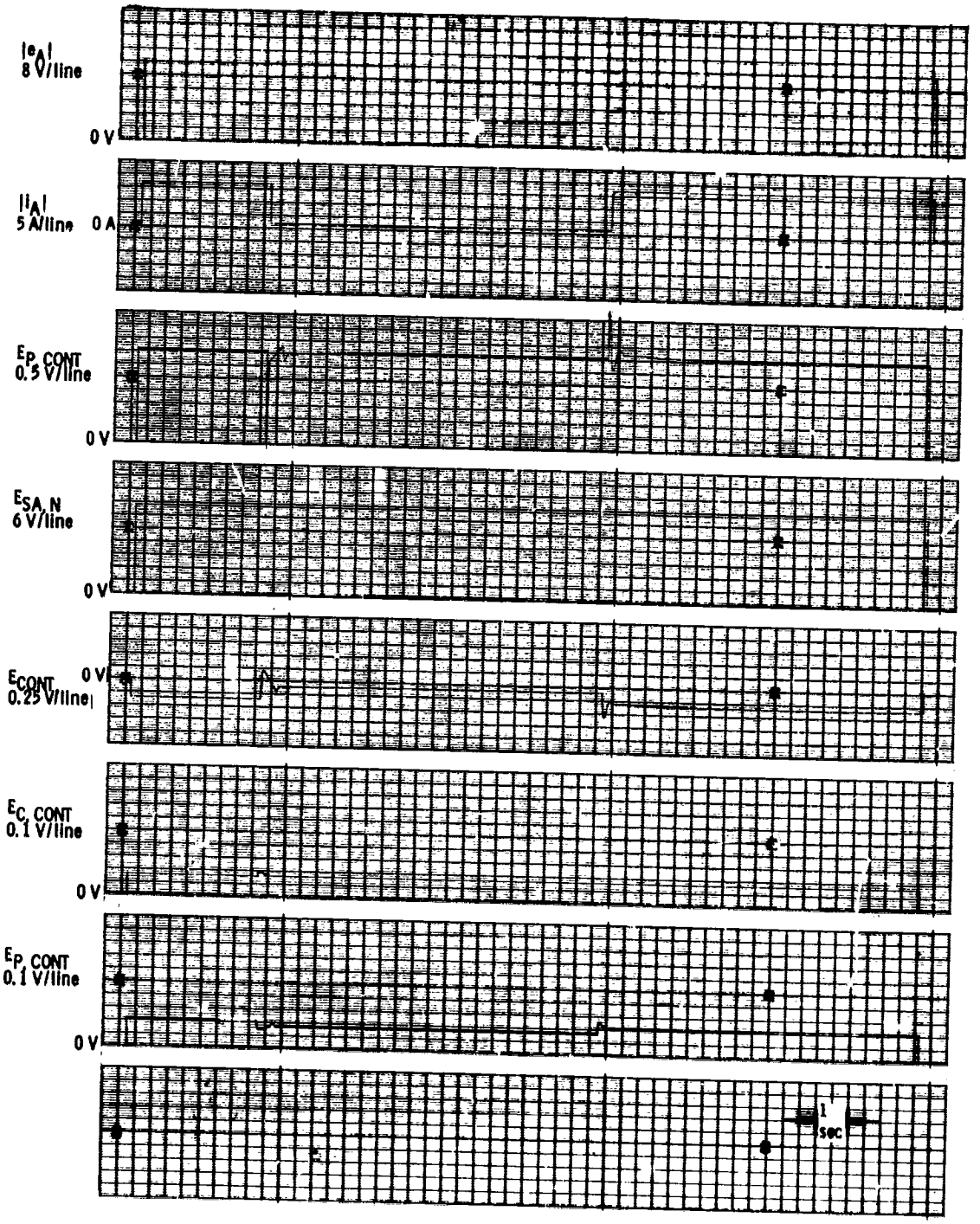

Figure 12. - Concluded.

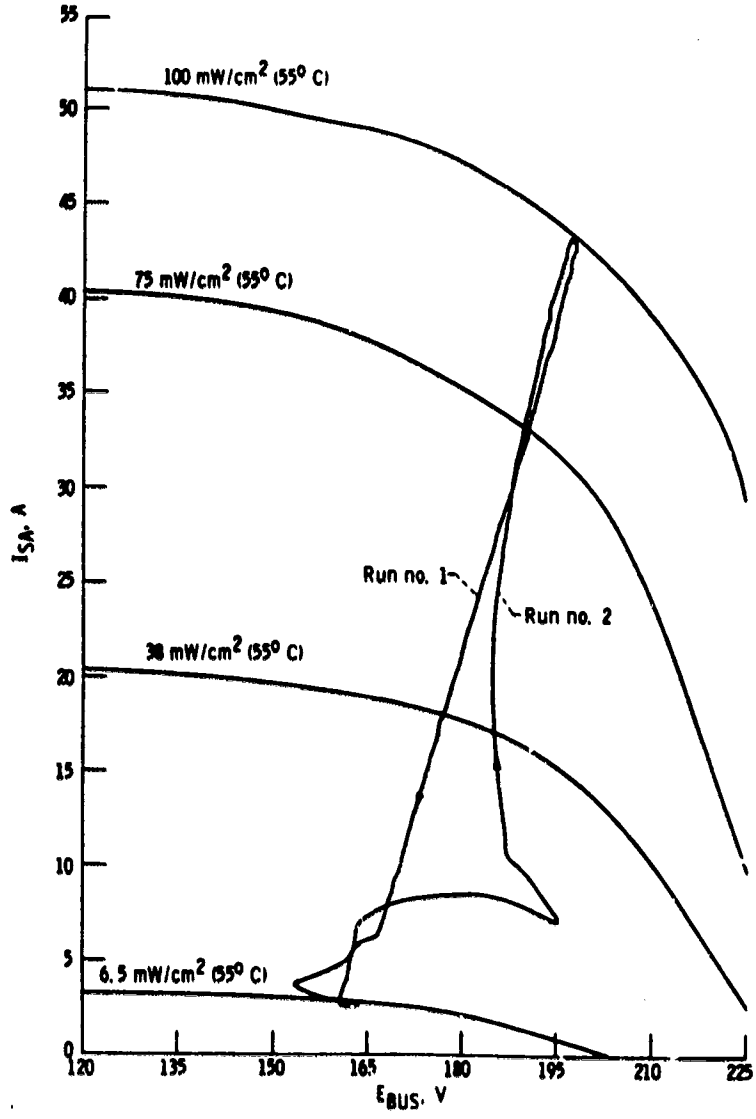

Figure 13. - Cloud cover and clear transients with basic BCC at 95 percent SOC.

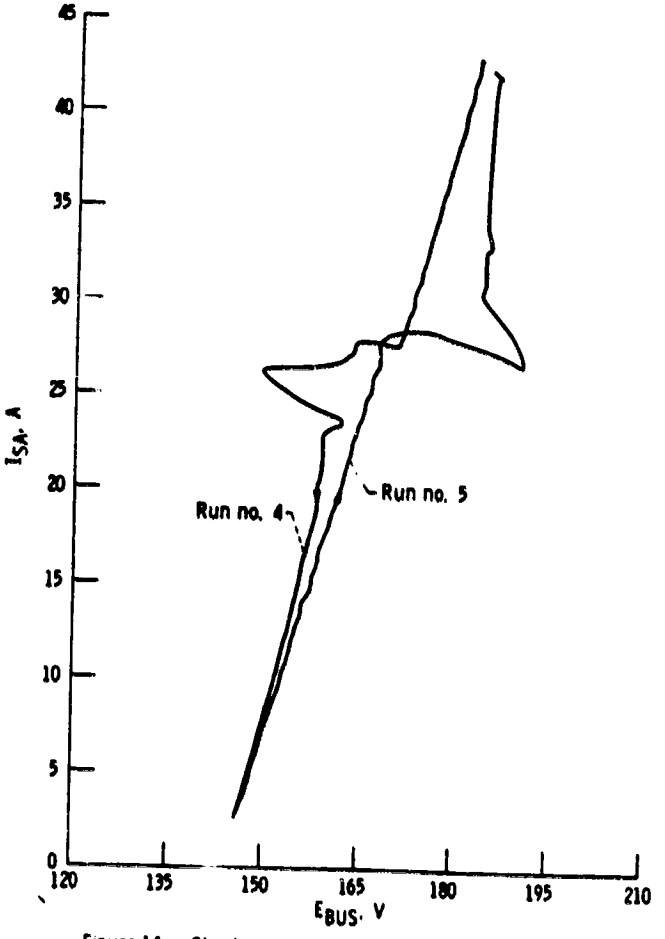

Figure 14. - Cloud cover and clear transients with basic BCC at 30 percent SOC.

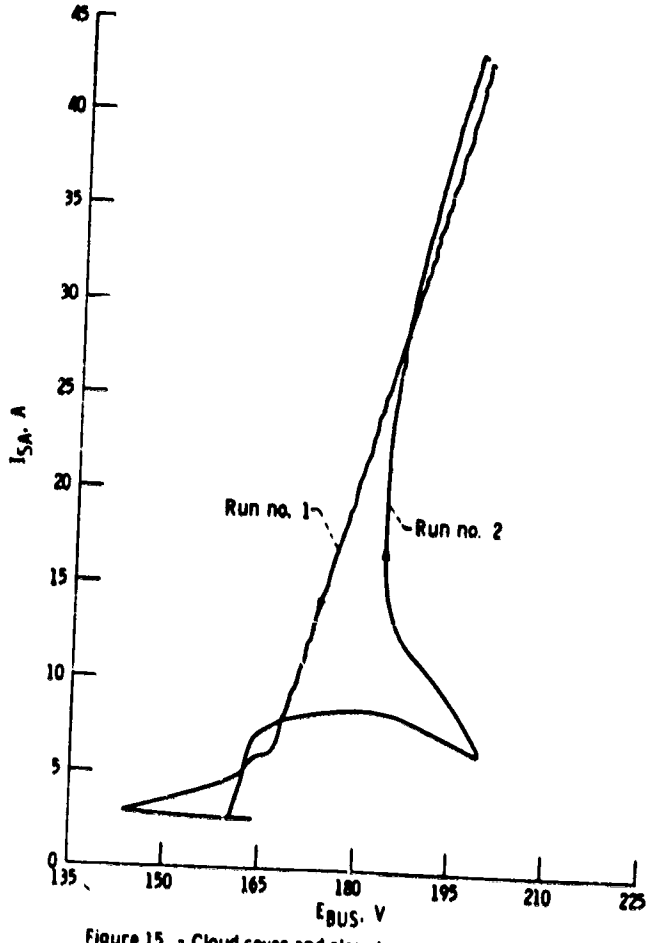

Figure 15. - Cloud cover and clear transients with 0.5 Hz filter characteristic at 95 percent SOC.

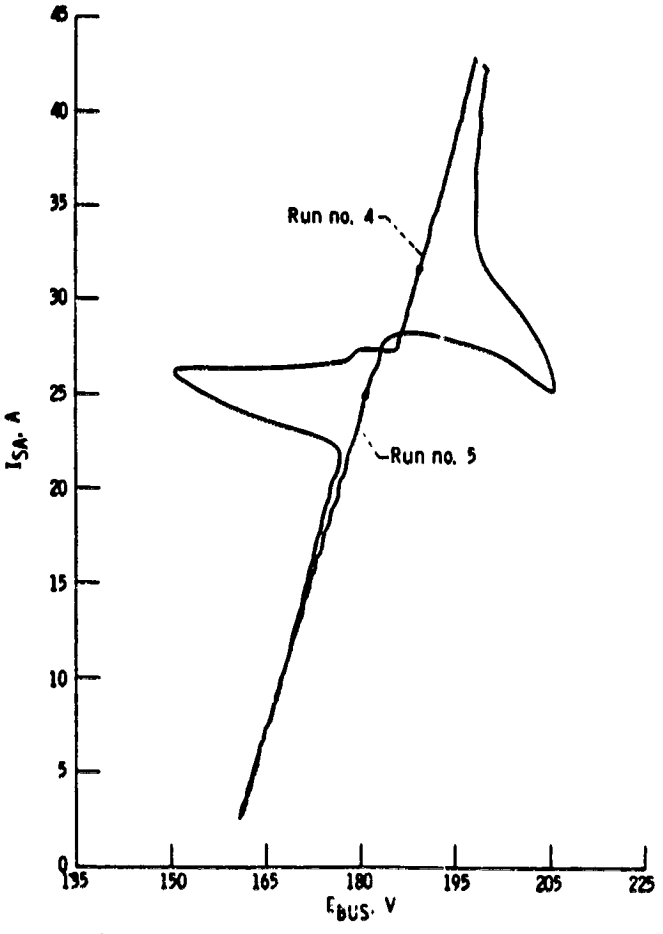

Figure 16. - Cloud cover and clear transients with 0.5 Hz filter characteristic at 30 percent SOC.

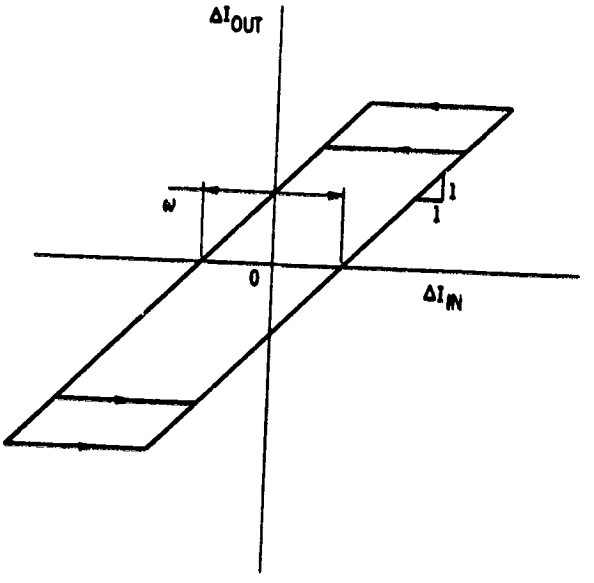

Figure 17. - Current measurement hysteresis characteristic.

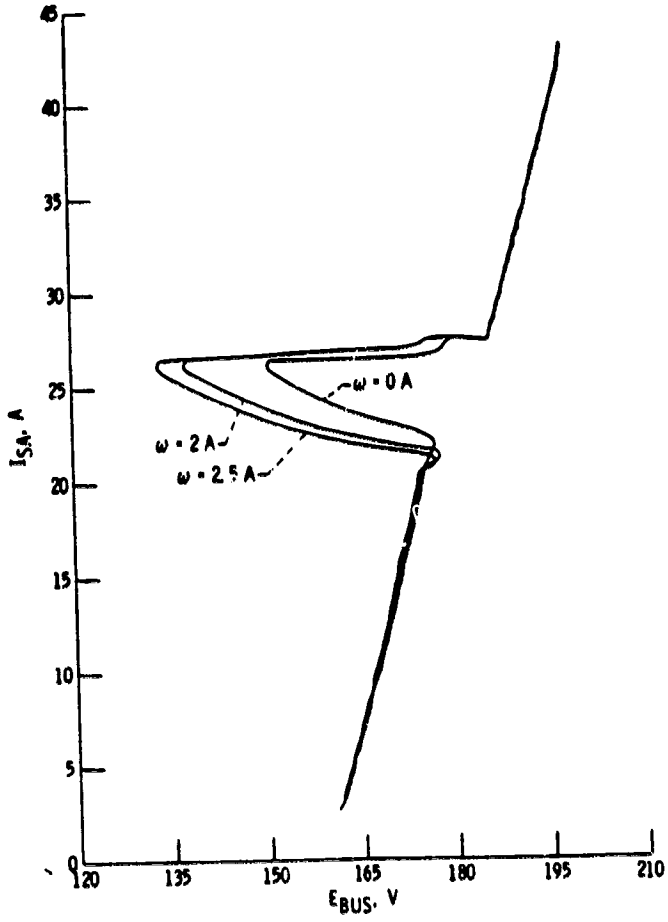

Figure 18. - Cloud cover transient with 0.5 Hz filter characteristic and varying hysteresis at 30 percent SOC.

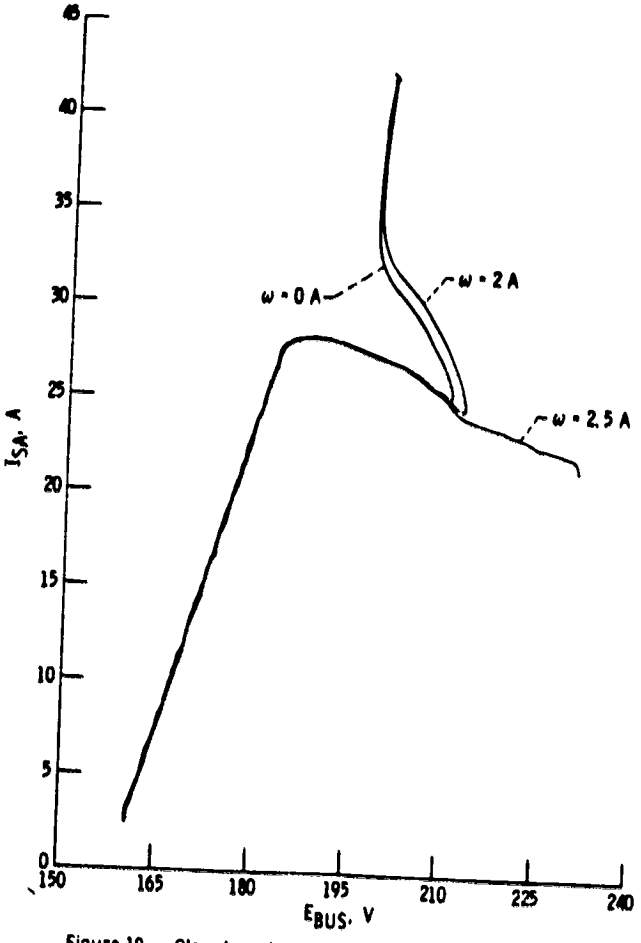

Figure 19. - Clear transient with 0.5 Hz filter characteristic and varying hysteresis at 30 percent SOC.

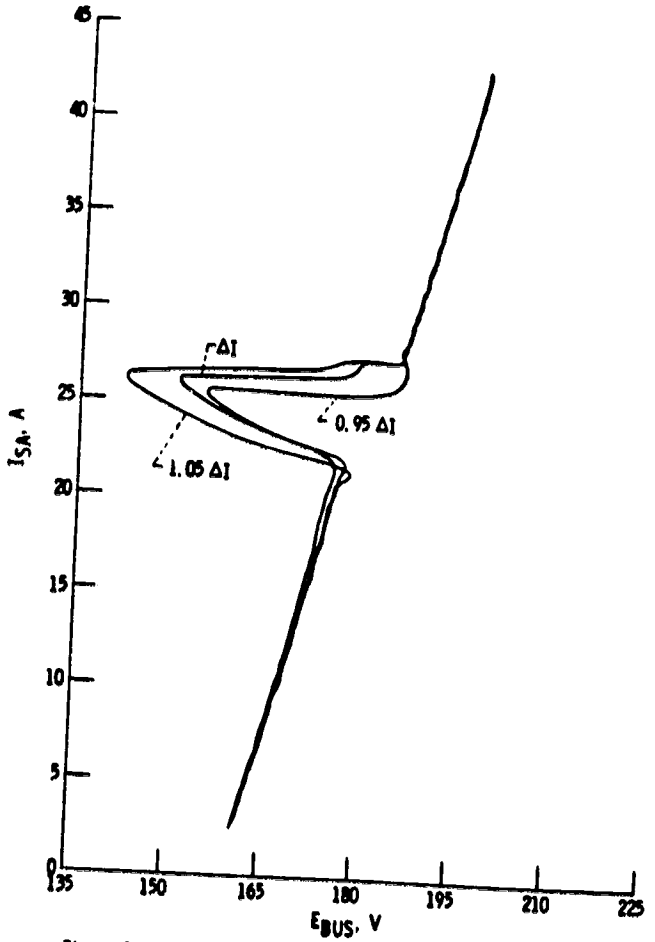

Figure 20. - Cloud cover transient with 0.5 Hz filter characteristic and various measurement errors at 30 percent SOC.

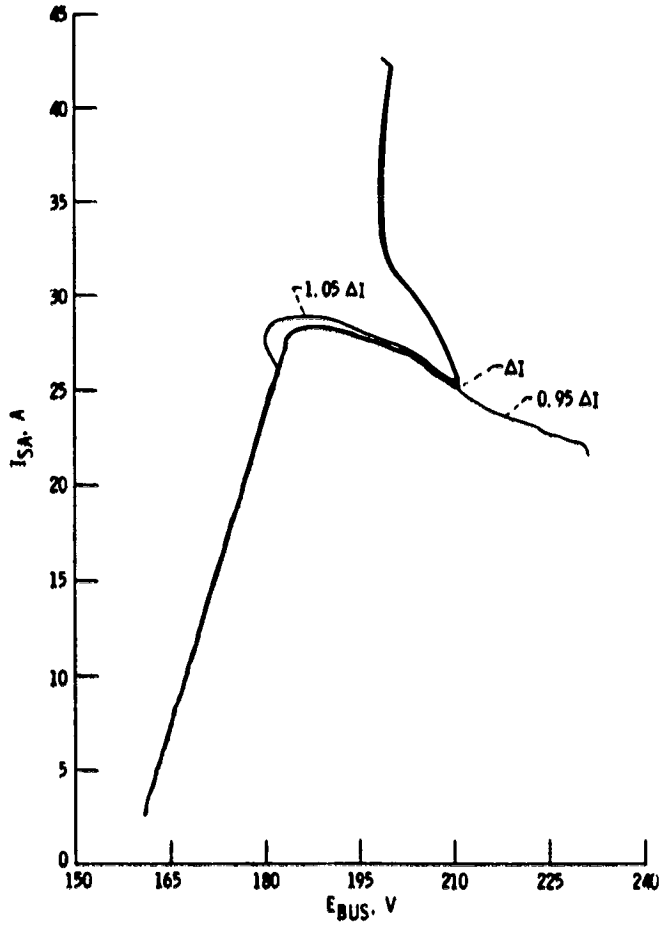

Figure 21. - Clear transient with 0.5 Hz filter characteristic and various measurement errors at 30 percent SOC.

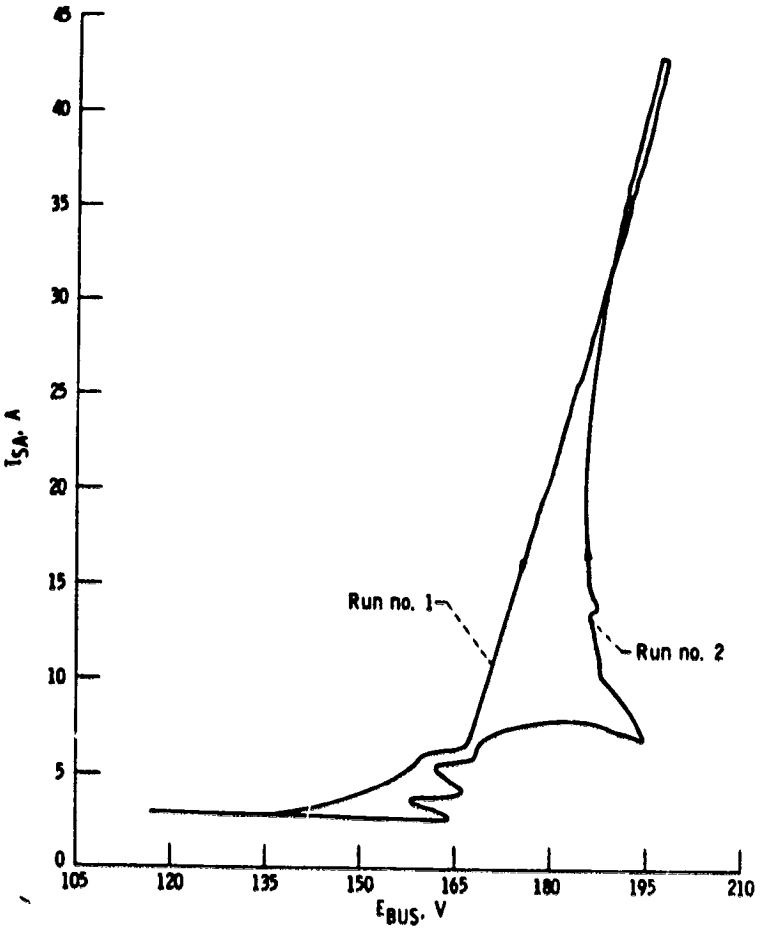

Figure 22. - Cloud cover and clear transients with updated BCC at 95 percent SOC.

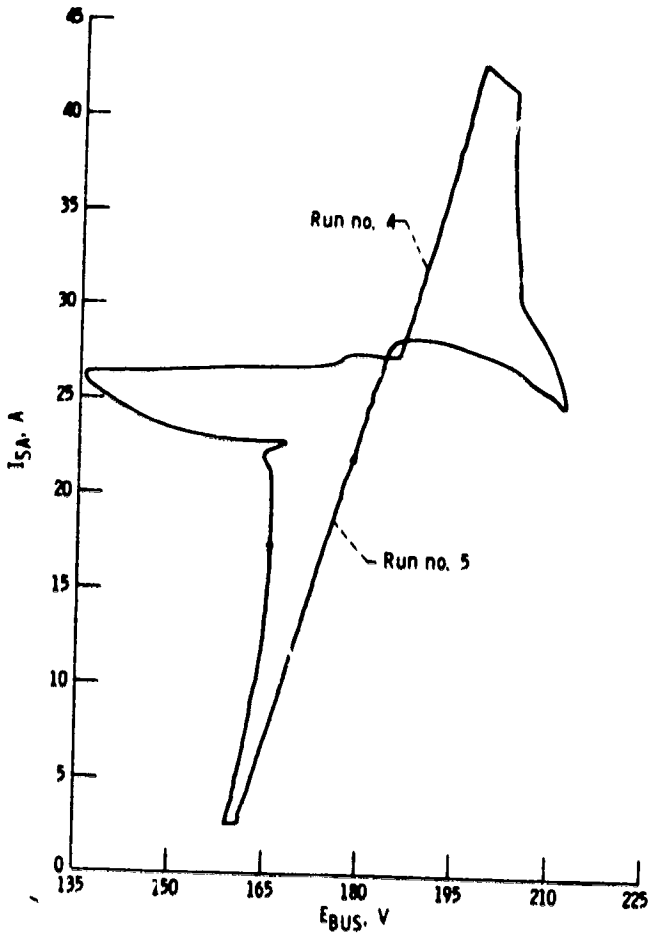

Figure 23. - Cloud cover and clear transients with updated BCC at 30 percent SOC.

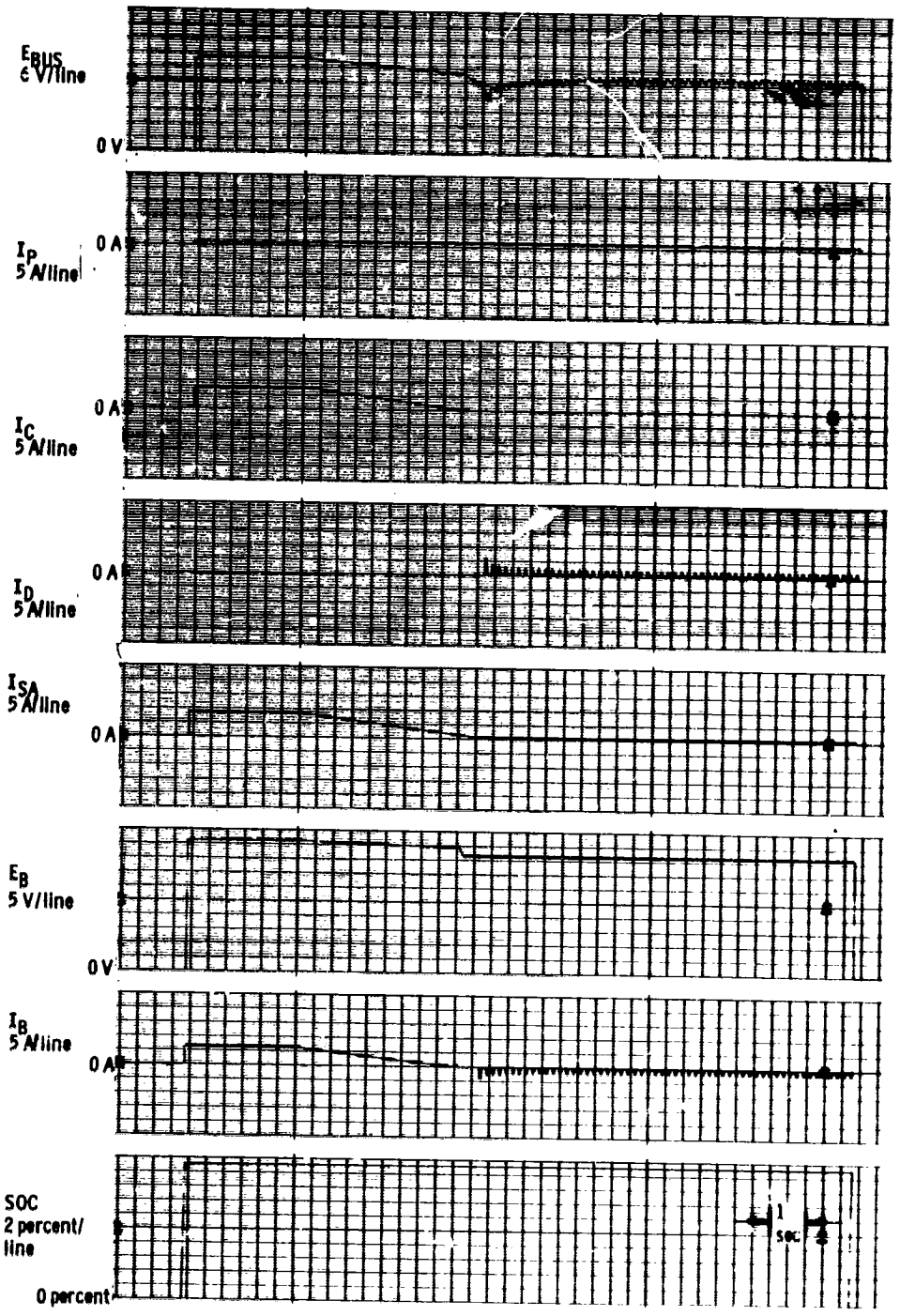

Figure 24. - Cloud cover transient with updated BCC at 95 percent SOC.

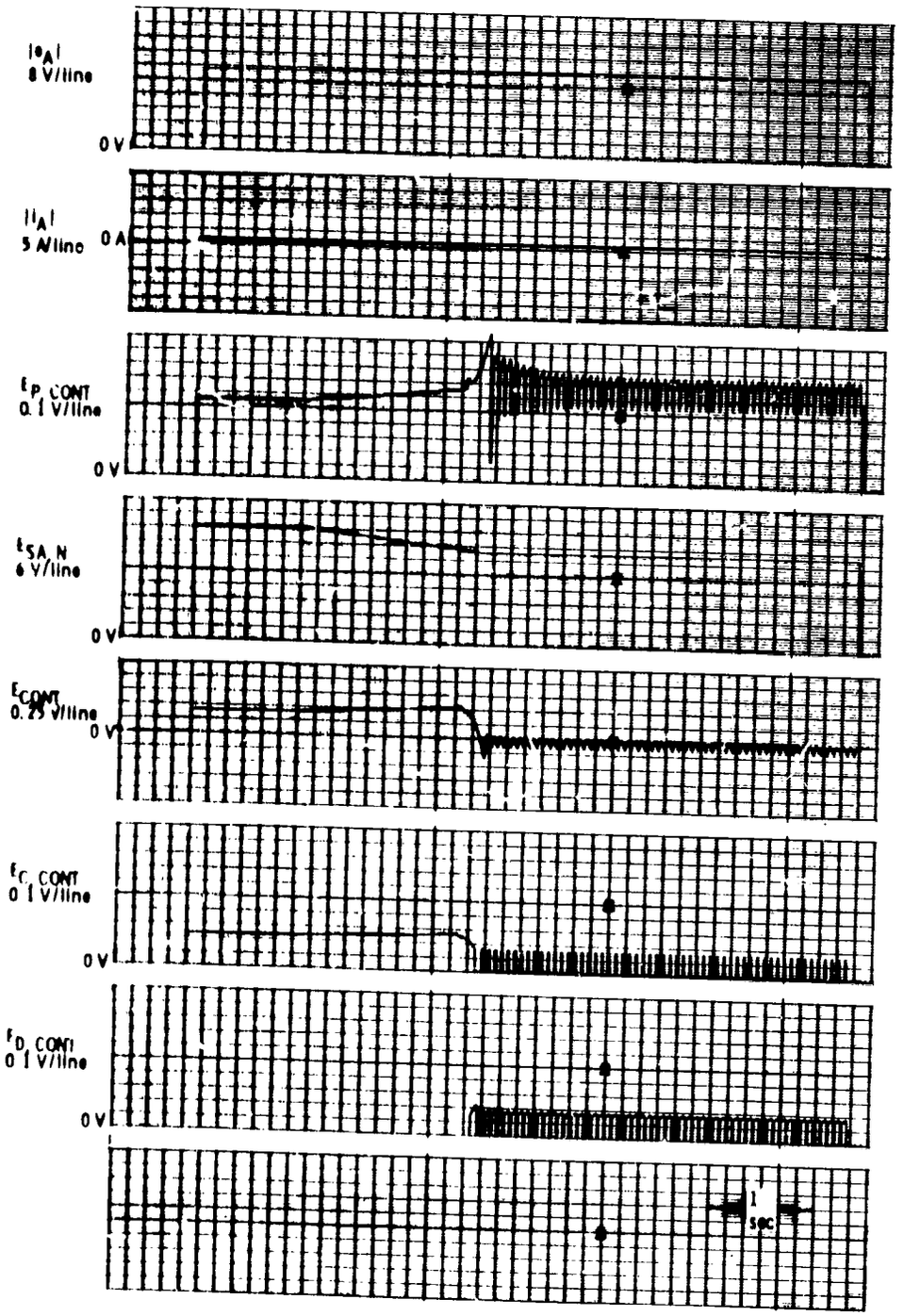

Figure 24. - Concluded.

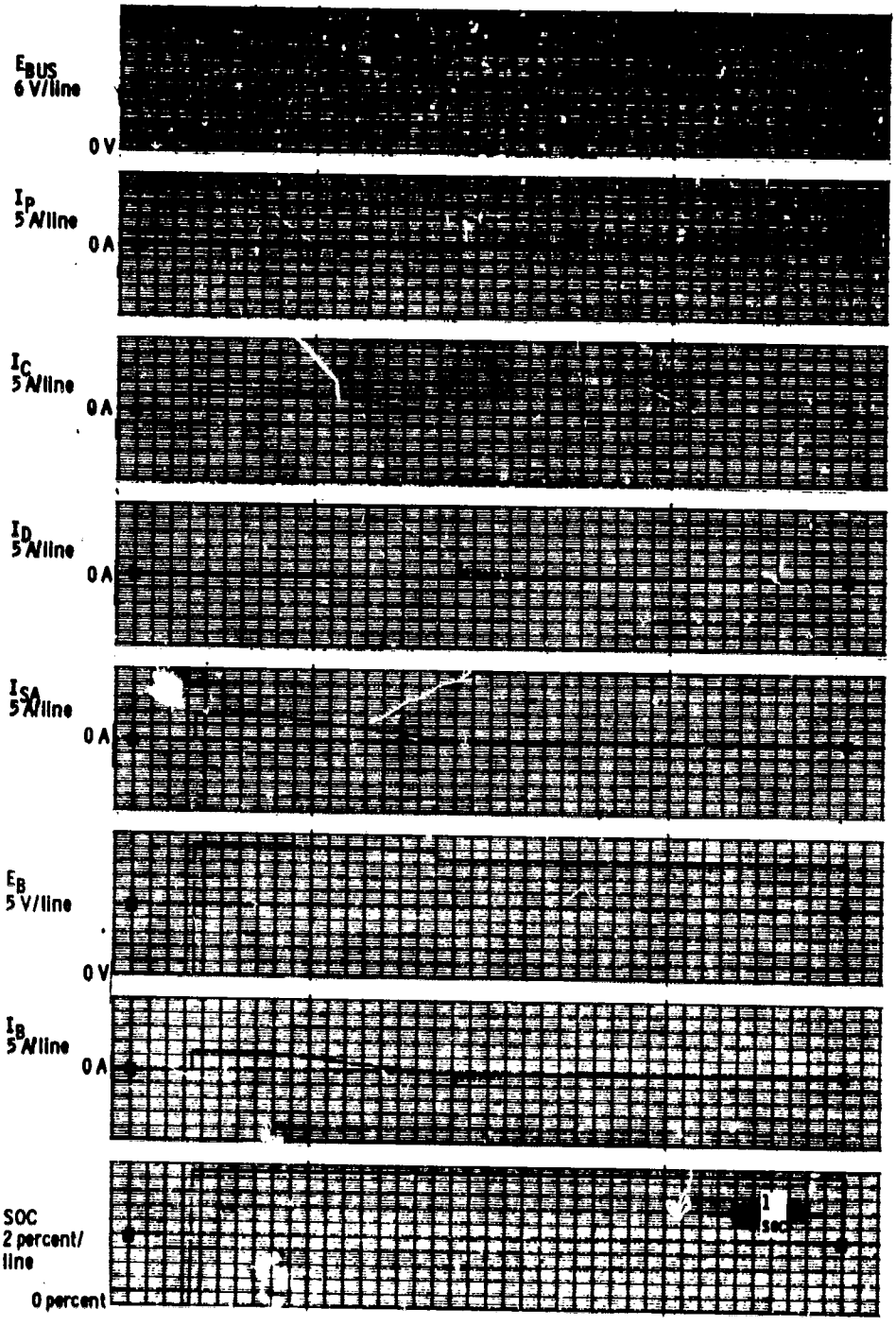

Figure 25. - Cloud cover transient with modified BCC at 95 percent SOC.

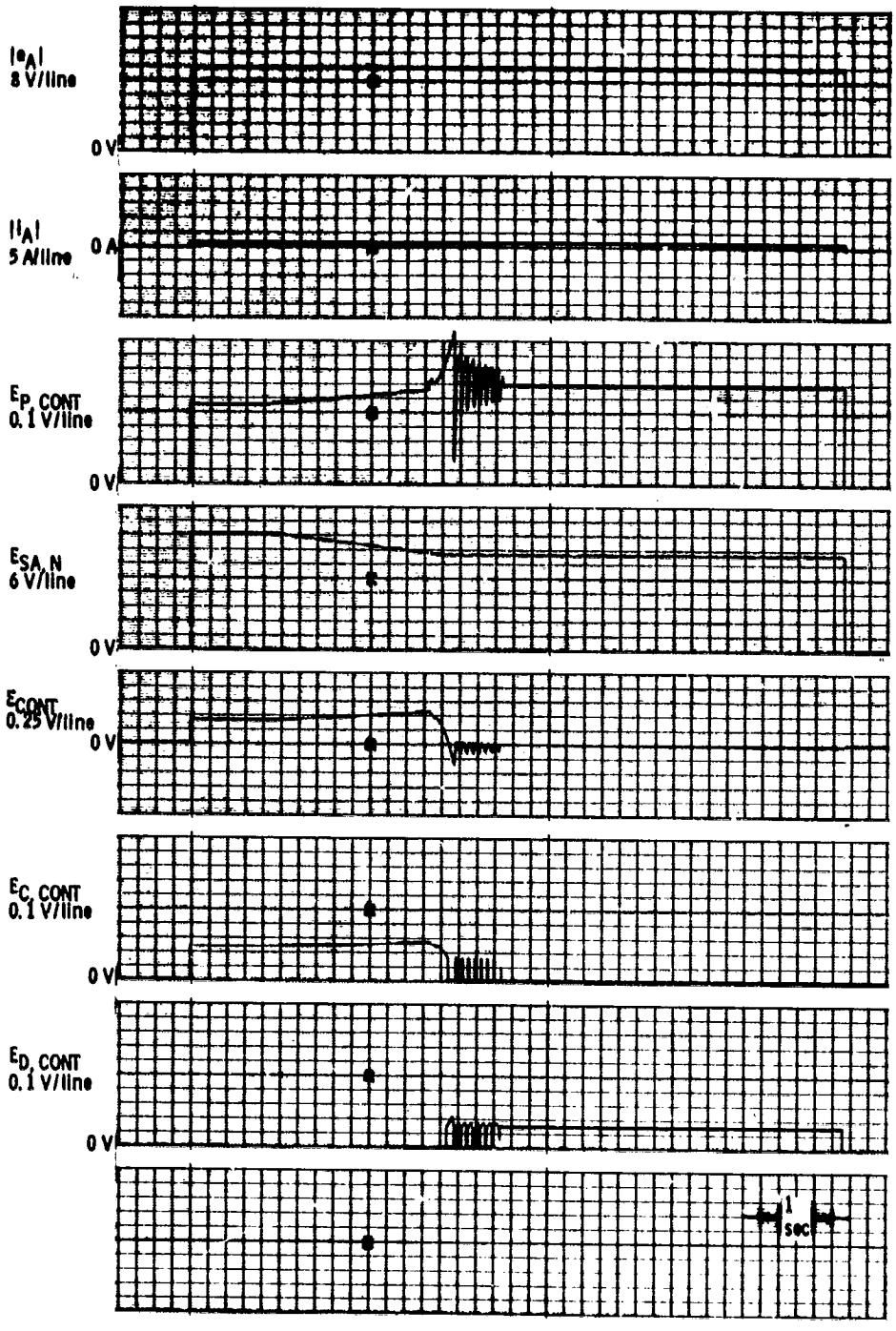

Figure 25. - Concluded.

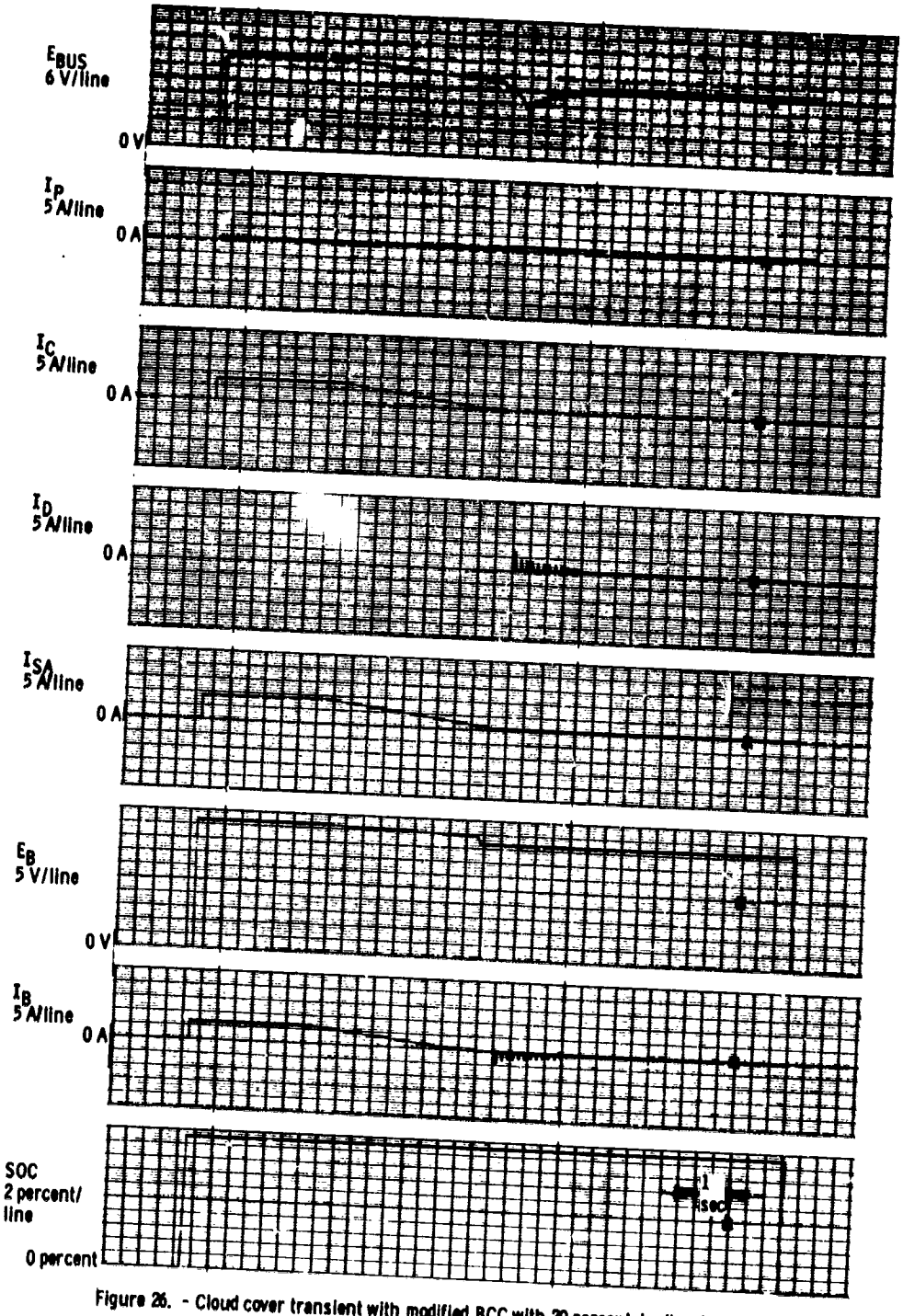

Figure 26. - Cloud cover transient with modified BCC with 20 percent deadband at 95 percent SOC.

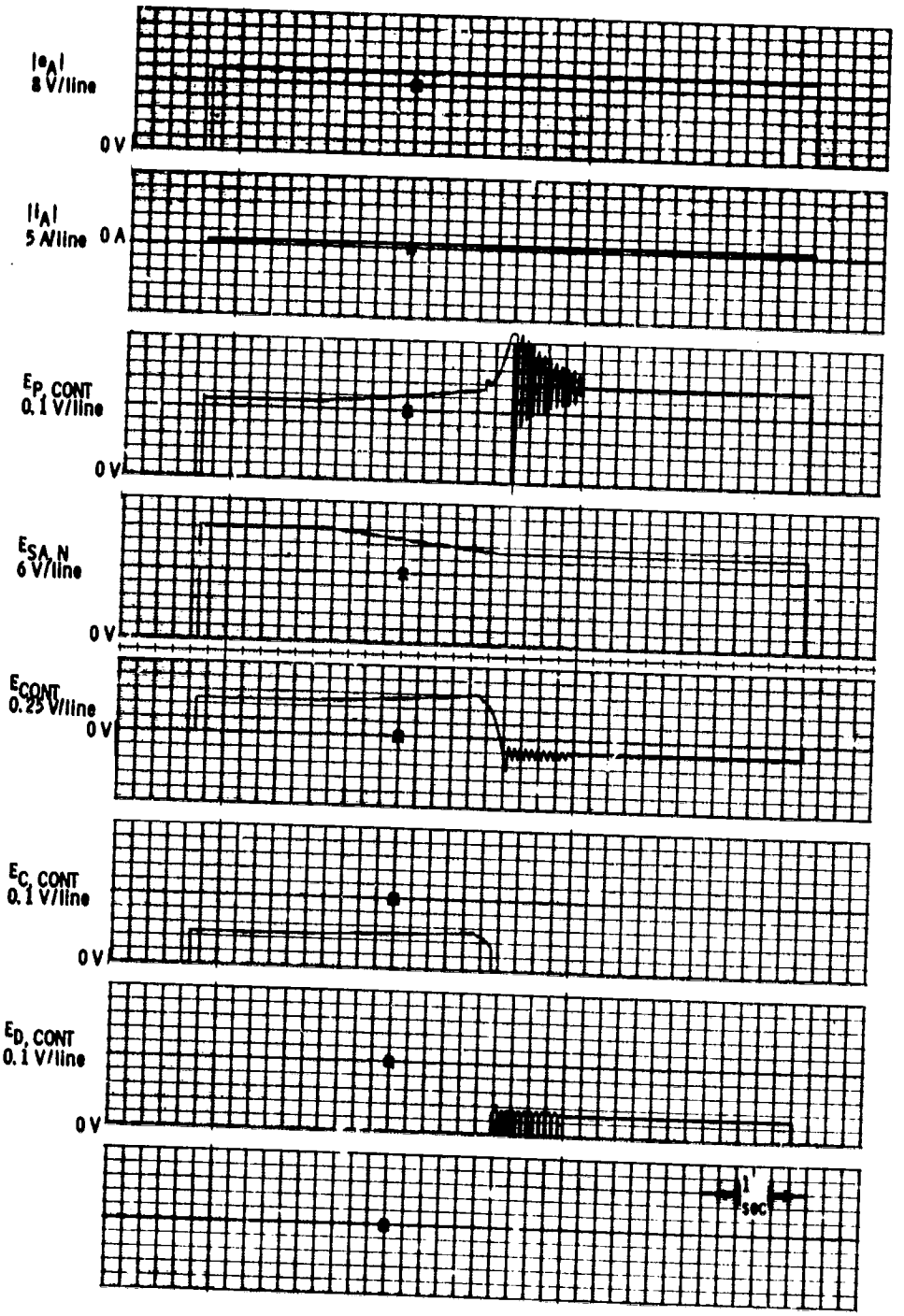

Figure 26. - Concluded.